NUCLEAR THEORY, Vol. 42 (2025)
eds. M. Gaidarov, N. Minkov, Heron Press, Sofia

Ab Initio Nuclear Physics: The bridge between "Heaven and Earth"

F. Sammarruca*, **T. Ajagbonna**, **P. Thapa**

University of Idaho, Moscow, Idaho, 83844-0903, USA

Abstract. The radial profile of a neutron star probes a very large range of densities, from the density of iron up to several times the density of saturated nuclear matter, and thus no theory of hadrons can be considered reliable if extended to those regions. We emphasize the importance of taking contemporary *ab initio* theories of nuclear and neutron matter as the baseline for any extension method, which will unavoidably involve some degree of phenomenology. We discuss how microscopic theory, on the one end, with causality and maximum-mass constraints, on the other, set strong boundaries to the high-density equation of state. We discuss polytropic continuations of the stellar matter equation of state as well as other parametrizations guided by speed of sound considerations.

1 Introduction

The large neutron skin in ^{208}Pb measured by PREX II, inconsistent with the result of CREX for the neutron skin of ^{48}Ca, has been attributed to the complexity of nuclear structure, see Ref. [1] and references therein. Here, we advance the point of view that the best strategy for "Connecting Heaven and Earth" [1] is found in *ab initio* theory, rather than attempts to reconcile the outcomes of PREX II and CREX.

A fully microscopic equation of state (EoS) up to central densities of the most massive stars – potentially involving phase transitions and non-nucleonic degrees of freedom – is not within reach. Nevertheless, neutron stars are powerful natural laboratories for constraining theories of the EoS [2–7]. One must be mindful of the theory's limitations and identify the best ways to extract and interpret information from observational constraints. Recently, detection of gravitational waves from merging of binary neutron star systems provided constraints on both their radius and tidal deformability.

Large Bayesian interference analyses have become popular as a tool to constrain the properties of neutron-rich matter. An example is Ref. [8], where the authors sample 15,000 EoSs, together with observational constraints and heavy ion collision (HIC) data. These analyses are important, but one must be careful about interpretation – relating HIC observables to parametrizations of the EoS is not a model-independent process. It is therefore not surprising that the authors

*To Rup, with everlasting love

of Ref. [8] find that the HIC constraints tend to prefer stiffer EOSs than those favored by astrophysical observations, and, we add, stiffer than those generated by *ab initio* theory. The reasons can be found in the phenomenological density functionals inspired by Quantum Hydrodynamics (QHD), often used to relate HIC observables to the EoS parameters. This point will be discussed in sec. 3.

Recent empirical determinations of the stellar matter EoS from data and observations have been reported in Refs. [9, 10]. When using sophisticated statistical techniques, it's important not to lose sight of basic physics arguments, such as the importance of a realistic description of few-body data. An extensive discussion on this point can be found in Ref. [11].

In this paper, keeping a firm foot in the microscopic theory – that is, with no adjustments of nuclear forces in the medium – we wish to illustrate *general features* of the EoS in different density regions, based only on theory (for normal to moderately above normal densities), and a few robust constraints, such as causality and the most recent maximum-mass constraints [12] (for high and super-high densities).

This paper is organized as follows. In sec. 2, we brifly review our theoretical ingredients, omitting lengthy details that have been published elsewhere. In sec. 3, we discuss various options for continuation of the EoS above the microscopic predictions. We also address the scenario where the conformal limit for the speed of sound in dense matter is satisfied. Our main takeaways are summarized in sec. 4.

2 Theoretical Framework

The theoretical framework we use to obtain the *ab initio* part of the equation of state has been published in detail elsewhere [13–15], and thus we will not repeat a lengthy presentation here. We will, however, briefly recall the spirit of chiral effective field theory (EFT), on which our nuclear forces are based. A comprehensive and detailed review of our theoretical tools can be found in Ref. [16].

2.1 Basic concepts in chiral EFT

Given an energy scale and degrees of freedom appropriate at that scale, an EFT comprises all interactions consistent with the symmetries that govern those degrees of freedom. For the nuclear problem, relevant degrees of freedom are pions (Goldstone bosons), nucleons, and $\Delta(1232)$ isobars. We use the delta-less chiral EFT. To begin with, one writes the most general Lagrangians describing all interactions between pions, nucleons, and pions with nucleons. Because pion interactions must vanish at zero momentum transfer and in the chiral limit, where the pion mass, m_π, goes to zero, the corresponding Lagrangian is expanded in powers of spatial derivatives or pion masses. From these Lagrangians, an infinite number of Feynman diagrams can be generated, which seems to render the theory unmanageable. The strategy is then to design a scheme for ordering the

diagrams according to their importance – the essence of Chiral Perturbation Theory (ChPT). Nuclear potentials are defined by the irreducible types among these graphs. (By definition, an irreducible graph is a diagram that cannot be separated into two by cutting only nucleon lines.) These graphs are then analyzed in terms of powers of Q, with $Q = p/\Lambda_b$, where p is generic for a momentum, (nucleon three-momentum or pion four-momentum), or the pion mass, and $\Lambda_b \sim m_\rho \sim$ 0.7 GeV (with m_ρ the mass of the ρ meson) is the breakdown scale [17]. Determining the power ν has become known as power counting.

2.2 Chiral orders and three-nucleon forces: Unresolved issues

While the predictions at N^{2}LO are fully *ab initio*, a warning is in place for current N^{3}LO calculations. As pointed out in Ref. [18], there is a problem with the regularized 3NF at N^{3}LO (and higher orders) in all present nuclear structure calculations. The N^{3}LO 3NFs currently in use are regularized by a multiplicative regulator applied to the 3NF expressions as derived from dimensional regularization. This approach leads to violation of chiral symmetry at N^{3}LO and destroys the consistency between two- and three-nucleon forces [18, 19]. Consequently, none of the current calculations that include 3NFs at N^{3}LO (and beyond) can be considered truly *ab initio*. An appropriate symmetry-preserving regulator [18] should be applied to the 3NF at N^{3}LO from Refs. [20, 21]. At the present time, reliable predictions exist only at N^{2}LO, NLO, and LO. However, for the few fully *ab initio* calculations, the precision at N^{2}LO is unsatisfactory. A first step towards deriving consistently regularized nuclear interactions in chiral EFT has

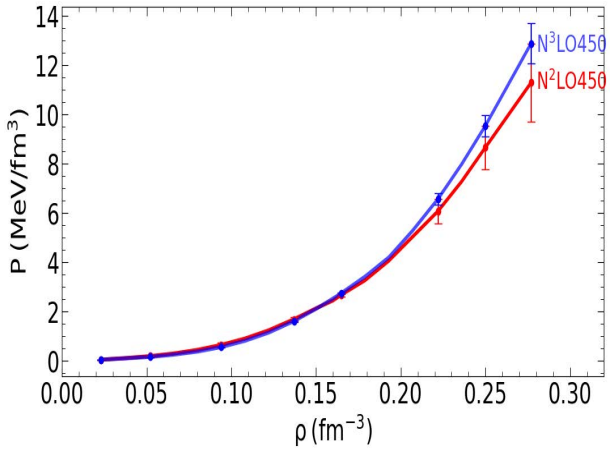

Figure 1. Pressure as a function of density in β-stable matter at N^{2}LO (red) and at N^{3}LO (blue), with the respective truncation errors. In both cases, the predictions are based on the high-quality NN potential of Ref. [24] and include all 3NFs required at the respective order.

been proposed in Refs. [22,23]. It requires the cutoff to be introduced already at the level of the effective Lagrangian. A path integral approach [22] can then be applied to the regularized chiral Lagrangian to derive nuclear forces through the standard power counting of chiral EFT.

Throughout the paper, we will show results at the (fully consistent) third order (N^2LO), and at the highest order which we have considered (fourth order, or N^3LO). In Figure 1, we show the pressure as a function of density in β-stable matter at N^2LO (red) and at N^3LO (blue), with the respective truncation errors. In both cases, the predictions are based on the high-quality nucleon-nucleon (NN) potential of Ref. [24] and include all 3NFs required at that order. For details on how our EoS are built, see, for instance, Refs. [13,15].

3 The Equation of State at High Density

It is important to emphasize that high-density EoS continuations are not meant to be a replacement for microscopic theories which, at this time, are not feasible in those regimes. Nevertheless, causality and maximum-mass constraints do pose considerable restrictions on the general features of the high-density EoS, as we discuss next.

3.1 Polytropic extensions

Up to this point, we constructed extensions using piecewise polytropes, which have the form:

$$P(\rho) = \alpha\Big(\frac{\rho}{\rho_0}\Big)^{\gamma}\,, \tag{1}$$

where ρ_0 is the density of saturated nuclear matter and γ is the adiabatic index. In the past, we accepted polytropes which can support a maximum mass of at least 2.01 $M_\odot$, to be consistent with the lower limit of the (2.08 $\pm$ 0.07) $M_\odot$ observation reported in Ref. [7] for the J0740+6620 pulsar, along with a radius estimate of (12.35 $\pm$ 0.75) km. The M(R) relations were obtained with piecewise combinations of two polytropes with different adiabatic index. Equations of state that cannot support a maximum mass of at least 2.01 $M_\odot$ (see above), are discarded, and solutions are cut at the central density where causality is violated [15]. The initial range we considered for the adiabatic index, γ, was approximately between 2.5 and 4.0, based on guidance from the literature, such as Ref. [25], where most of the EoS available from theory or phenomenology were fitted with polytropes.

Currently, the maximum-mass constraint must account for the record-setting PSR J0952-0607, the heaviest neutron star found to date, at (2.35 $\pm$ 0.17) $M_\odot$ [12]. We point out that this measurement was based on optical lightcurve modeling and may not be as accurate as those based on radio observations. For instance, for PSR J2215+5135, the optical lightcurve modeling suggests a mass of (2.27$\pm$ 0.17) $M_\odot$ [26], while recent radio observations yield a significantly smaller

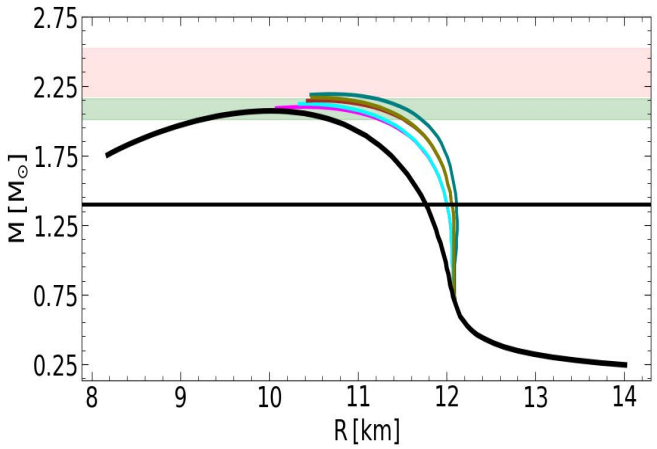

Figure 2. Several M(R) relations. The curves in color are obtained from a sequence of two polytropes with adiabatic indices given in Table 1. The black curve is obtained with a single parametrization in terms of the speed of sound, as in Eq. (7).

value of $(1.98 \pm 0.08)\ M_\odot$ [27]. The analysis in Ref. [28] found a maximum mass of $(2.25 \pm 0.07)\ M_\odot$ for a non-rotating neutron star.

We explored different piecewise parametrizations of the high-density EoS that preserve causality, while supporting masses at least as high as $2.2\ M_\odot$. We emphasize that *ab initio* predictions and most of the terrestrial constraints point to a soft symmetry energy at normal density, while the maximum mass constraint has moved to larger values. These considerations provide important guidance when building the phenomenological part of the EoS. While checking different polytropic combinations, we made the observation that the "best" combination (with regard to preserving causality while satisfying maximum-mass constraints) consists of a relatively stiff polytrope attached to the microscopic piece of the EoS, followed by a second, softer polytrope. In Figure 2, the colorful curves are from selected EoS that generate maximum masses of about 2.1 to 2.2 solar masses and are consistent with causality. Table 1 provides more information about these cases.

Table 1. Description of the M(R) relations in Figure 2

curve color	Γ_1	Γ_2	$M_{max}/M_\odot$	$R_{1.4}$ (km)
magenta	3.1	2.7	2.10	12.00
cyan	3.1	2.8	2.12	12.00
brown	3.2	2.7	2.15	12.06
olive	3.2	2.8	2.17	12.06
green	3.3	2.7	2.19	12.11

Although polytropic extension is a very general and popular method, alternative parametrizations of the high-density EoS offer desirable features [29,30], such as those in terms of the speed of sound, as we discuss next.

3.2 Continuations involving the speed of sound in stellar matter

We find that, for the purpose of achieving high maximum masses while respecting causality at any density, a better solution is to combine a relatively steep polytrope followed by a parametrization obtained from Eqs. (2–7), which will maintain causality by construction. The resulting $M(R)$ curves are shown in Figure 3 for both N^{3}LO (blue) and N^{2}LO (red). For the dashed curves, the first extension is done with a polytrope with γ = 3.3, followed by pressure values given by Eq. (7) with the speed of sound as in Eq. (2). The solid curves (same color convention) have been obtained with γ = 3.8, a value beyond which the EoS begins to violate causality. Table 2 displays the maximum mass, its radius, the central density, and the radius of the canonical mass neutron star, for the curves in Figure 3. We recall that the radius of a 1.4 $M_\odot$ is sensitive to the pres-

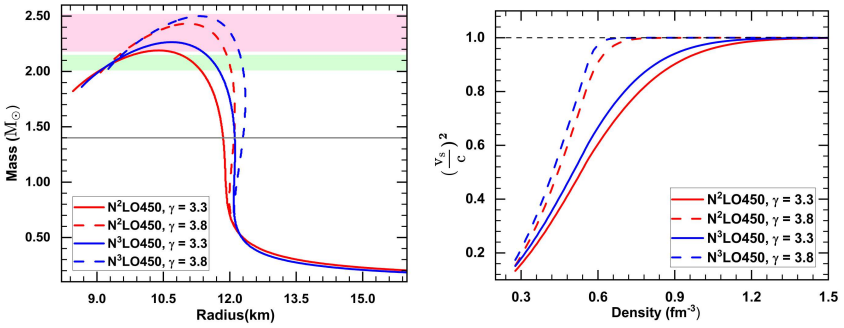

Figure 3. Left: M(R) curves at fourth order (N^{3}LO, blue) and at third order (N^{2}LO, red) of ChPT. Dashed curves: the first extension is done using a polytrope with γ = 3.3, followed by pressure values given by Eq. (7) together with Eq. (2); Solid curves: obtained with γ = 3.8, a value beyond which the EoS begins to violate causality. Right: Dimensionless speed of sound squared corresponding to the curves on the left. Same color and pattern conventions.

Table 2. Some neutron star properties corresponding to the red and the blue M(R) relations shown in Figure 3

γ	chiral order	$M_{max}/M_\odot$	$R_{M_{max}}(km)$	$\rho_c(fm^{-3})$	$R_{1.4}$ (km)
3.3	N^{2}LO	2.19	10.39	1.09	11.84
	N^{3}LO	2.27	10.68	1.03	12.11
3.8	N^{2}LO	2.43	11.06	0.93	12.09
	N^{3}LO	2.50	11.32	0.88	12.30

sure at normal densities and thus it can pose constraints on microscopic theories of the EoS at those densities where such theories are applicable.

3.2.1 Causality without conformal limit

We parametrize the speed of sound as

$$\left(\frac{v_s}{c}\right)_i^2 = 1 - c_1 exp\Big[-\frac{(\rho_i - c_2)^2}{w^2}\Big] , \tag{2}$$

where w is the width of the Gaussian curve, and the constants c_1 and c_2 are determined from continuity of the speed of sound and its derivative at the threshold density. Assigning $i = 0$ to values at threshold (the density at which the EoS parametrization has to be attached to the previous piece), we write

$$\rho_i = \rho_{i-1} + \Delta\rho , \tag{3}$$

$$\epsilon_i = \epsilon_{i-1} + \Delta\epsilon , \tag{4}$$

and

$$\Delta\epsilon = \Delta\rho \frac{\epsilon_{i-1} + P_{i-1}}{\rho_{i-1}} , \tag{5}$$

where we have used the basic thermodynamic relation between internal pressure and energy density,

$$P(\rho) = \rho^2 \frac{d}{d\rho}\left(\frac{\epsilon}{\rho}\right) . \tag{6}$$

The pressure above the threshold is then:

$$P_i = \left(\frac{v_s}{c}\right)_{i-1}^2 \Delta\epsilon + P_{i-1} . \tag{7}$$

3.2.2 Implementing the conformal limit

In the QCD limit of deconfined quarks in the presence of asymptotic freedom, quarks should behave like free fermions. Some perturbative QCD calculations [31] support the conformal limit, $(v_s/c)^2 = 1/3$. We observed that an EoS that's sub-conformal at all densities (that is, Eq. (2) with the asymptotic limit replaced by 1/3), cannot generate sufficiently large masses. On the other hand, the speed of sound can be asymptotically conformal and non-monotone. A scenario where the speed of sound peaks around few to several times nuclear density and then falls back to approach the QCD limit for deconfined quark matter would signify some sort of phase transition with the conformal limit reached well beyond central densities of the heaviest observed neutron stars. The superconformality condition, $\left(\frac{v_s}{c}\right)^2 > 1/3$, satisfied *on the average* in neutron stars may have fundamental implications on the trace of the energy-momentum tensor at the center of rotating neutron stars [32].

Here, we will explore parametrizations where the speed of sound is consistent with the conformal limit as the density approaches infinity. This can be simulated adding a second, skewed gaussian function to Eq. (2), and of course changing the asymptotic value to 1/3:

$$\Big(\frac{v_s}{c}\Big)^2_i = \frac{1}{3} - c_1 \exp\Big[-\frac{(\rho_i - c_2)^2}{w^2}\Big] + c_3 \exp\Big[-\frac{(\rho_i - c_4)^2}{w_2^2}\Big]\Big[1 + \mathrm{erf}\Big(c_5 \frac{(\rho_i - c_4)}{w_2}\Big)\Big]. \quad (8)$$

We solve for c_1 and c_2 as done above, matching Eq. (8) and its derivative to the values at threshold, within a chosen parameter space for the remaining three coefficients, c_3, c_4, c_5. The widths w and w_2 are obtained by normalizing both gaussians in the standard way. Clearly, this procedure can provide a large number of possibilities, not all physically acceptable. We observed that the roots, c_1 and c_2, converge easily within limited ranges for the free parameters: $c_3 \approx [0, 1]$, $c_4 \approx [1, 4] fm^{-3}$, $c_5 \approx [-50, 50]$. In fact, the roots tend to cluster around a few pairs of c_1, c_2 values, weakly sensitive to the large variations in c_5, and only moderately sensitive to variations of c_3 and c_4. As a consequence, our selected parametrizations produce very similar M(R) results. A representative case is shown by the green curves on the left-hand side of Figure 4, where we have chosen a polytropic index of 3.5 to ensure that the new curves would stand out in between the other two sets from Figure 3. The corresponding curves for the dimensionless speed of sound are seen to approach the conformal limit on the right-hand side of Figure 4.

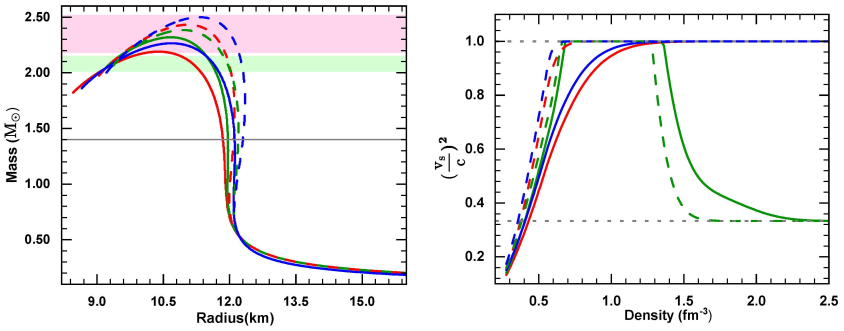

Figure 4. Left: M(R) curves at fourth order (N^3LO, blue) and at third order (N^2LO, red) of ChPT. Dashed curves: the first extension is done using a polytrope with γ = 3.3, followed by pressure values given by Eq. (7) together with Eq. (2); Solid curves: obtained with γ = 3.8, a value beyond which the EoS begins to violate causality. Right: Dimensionless speed of sound squared corresponding to the curves on the left. Same color and pattern conventions.

Implementing the conformal limit at all densities would not allow sufficiently large masses. Maximum masses as large as those recently observed require a rapid rise of the pressure soon after the first matching point.

4 Conclusion

The intrinsic and strong relation between the EoS and the maximum mass of a neutron star sequence is a remarkable feature. In fact, knowledge of one is essential to access the other. In our observations, the maximum-mass constraint moving to higher values, together with the causality requirement at any density, poses significant restrictions on the high-density EoS. The softness of the microscopic predictions at normal density brings up the need for a (first) steeper extension. A scenario such as the one we have described, where the first part of a piecewise extension needs to become stiffer in order to support current maximum mass constraints, while the next piece must soften to maintain causality, is consistent with evolving maximum-mass constraints. A non-monotone behavior, where the speed of sound peaks around few to several times nuclear density and then falls to approach the QCD limit for deconfined quark matter at very high density, would signify that phase transitions and/or new species (which can occupy their lowest energy states), begin to appear only at super-high densities. On the other hand, an EoS where the speed of sound is subconformal everywhere cannot generate sufficiently high maximum masses.

Acknowledgements

I am deeply grateful to the Organizers for the opportunity to participate remotely. This work was supported by the U.S. Department of Energy under Award No. DE-FG02-03ER41270.

References

[1] J. Mammei, F.J. Fattoyev, *Nucl. Phys. News* **34(2)** (2024) 11-15.
[2] B.P. Abbott et al., *Phys. Rev. Lett.* **119** (2017) 161101.
[3] B.P. Abbott et al., *Astrophys. J. Lett.* **848** (2017) L12.
[4] B.P. Abbott et al., *Phys. Rev. Lett.* **121** (2018) 161101.
[5] B.P. Abbott et al., *Phys. Rev. X* **9** (2019) 031040.
[6] M.C. Miller et al., *Astrophys. J. Lett.* **887** (2019) L24.
[7] M.C. Miller et al., *Astrophys. J. Lett.* **918** (2021) L28.
[8] S. Huth et al., *Nature* **606** (2022) 276.
[9] C.Y. Tsang et al., *Nature Astron.* **8** (2024) 328.
[10] P.J. Davis et al., *Astronomy & Astrophysics* **687** (2024) A44.
[11] F. Sammarruca, *Symmetry* **16** (2024) 34.
[12] R.W. Romani, D. Kandel, A.V. Filippenko, T.G. Brink, W. Zheng, *Astrophys. J. Lett.* **934** (2022) L18.
[13] F. Sammarruca, R. Millerson, *Phys. Rev. C* **104** (2021) 034308.

[14] F. Sammarruca, R. Millerson, *Phys. Rev. C* **104** (2021) 064312.
[15] F. Sammarruca, R. Millerson, *Universe* **8** (2022) 133.
[16] R. Machleidt, F. Sammarruca, *Prog. Part. Nucl. Phys.* **137** (2024) 104117.
[17] R.J. Furnstahl, N. Klco, D.R. Phillips, S. Wesolowski, *Phys. Rev. C* **92** (2015) 024005.
[18] E. Epelbaum, H. Krebs, P. Reinart, *Front. Phys.* **8** (2020) 98.
[19] E. Epelbaum, H. Krebs, P. Reinart, In: *Handbook of Nuclear Physics*, edited by I. Tanihata, H. Toki, T. Kajino (Springer, Singapore, 2023).
[20] V. Bernard, E. Epelbaum, H. Krebs, Ulf-G Meissner, *Phys. Rev. C* **77** (2008) 064004.
[21] V. Bernard, E. Epelbaum, H. Krebs, Ulf-G Meissner, *Phys. Rev. C* **84** (2011) 054001.
[22] H. Krebs, E. Epelbaum, arXiv:2311.10893 [nucl-th]
[23] H. Krebs and E. Epelbaum, arXiv:2312.13932 [nucl-th]
[24] D. R. Entem, R. Machleidt, and Y. Nosyk, *Phys. Rev. C* **96** (2017) 024004
[25] J. S. Read, B. D. Lackey, B. J. Owen, and J. L. Friedman, *Phys. Rev. D* **79** (2009) 124032
[26] M. Linares, T. Shahbaz, and J. Casares, *ApJ* **859** (2018) 54
[27] A. G. Sullivan and R. W. Romani, arXiv:2405.13889 [astro-ph.HE].
[28] Y.-Z. Fan et al., arXiv:2309.12644v2 [astro-ph.HE].
[29] A. Kanakis-Pegios, P.S. Koliogiannis, C.C. Moustakidis, *Symmetry* **13** (2021) 183.
[30] I. Tews, J. Carlson, S. Gandolfi, S. Reddy, *Astrophys. J.* **860** (2018) 149.
[31] L. Brandes, W. Weise, N. Kaiser, *Phys. Rev. D* **107** (2023) 014011.
[32] R.F.P. Mendes, C.F. Sodré, F.T. Falciano, *Phys. Rev. D* **110** (2024) 104027.